

Dual-tool multiplexing model of parallel computer controlled optical surfacing

XIAOLONG KE,^{1,2} TIANYI WANG,³  HEEJOO CHOI,^{1,4} WESLIN PULLEN,¹ LEI HUANG,³ 
MOURAD IDRIS,³ AND DAE WOOK KIM^{1,4,5,*}

¹James C. Wyant College of Optical Sciences, The University of Arizona, 1630 E. University Blvd., P.O. Box 210094, Tucson, Arizona 85721-0094, USA

²School of Mechanical and Automotive Engineering, Xiamen University of Technology, Xiamen 361024, China

³National Synchrotron Light Source II (NSLS-II), Brookhaven National Laboratory, PO Box 5000, Upton, New York 11973, USA

⁴Large Binocular Telescope Observatory, University of Arizona, Tucson, Arizona 85721, USA

⁵Department of Astronomy and Steward Observatory, University of Arizona, 933 N. Cherry Ave., Tucson, Arizona 85721, USA

*Corresponding author: dkim@optics.arizona.edu

Received 5 August 2020; revised 29 September 2020; accepted 17 October 2020; posted 19 October 2020 (Doc. ID 404575); published 24 November 2020

Fabrication of large optics is a time-consuming process and requires a vast investment in manpower and financial resources. Increasing the material removal rate of polishing tools and minimizing dwell time are two common ways of reducing the processing time. Indeed, the polishing efficiency can be further improved if multiple tools are used at the same time. In this Letter, we propose a dual-tool deterministic polishing model, which multiplexes the dwell time and optimizes the run parameters of two polishing tools simultaneously. The run velocities of the two tools are coordinated by boundary conditions with a velocity adjustment algorithm, and the corresponding polishing paths are studied. We demonstrate this model with a simulation of polishing one segment of the Giant Magellan Telescope, where, with the proposed dual-tool multiplexing, the processing time of an $\varnothing 8.4$ m mirror has been reduced by 50.54% compared with that using two tools in a sequential schedule. © 2020 Optical Society of America

<https://doi.org/10.1364/OL.404575>

Due to the large size and the ever-increasing requirement on accuracy, fabrication of large optics becomes an extremely time-consuming process. For example, the Giant Magellan Telescope (GMT) [1], one of the world's largest telescopes, consists of seven segments, each of which is an $\varnothing 8.4$ m monolithic mirror. Polishing each segment to the specified accuracy, i.e., 20 nm root mean square (RMS) figure error, consumed about one year.

Increasing the material removal rate [2–6] is one straightforward way to save time. As shown in Fig. 1, a $\varnothing 1.2$ m stressed lap and a non-Newtonian lap have been used in the Large Synoptic Survey Telescope (LSST) and GMT polishing system to ensure adequate removal [2,7]. Similarly, the largest Zeeko-classic polishing machine equipped with a $\varnothing 320$ mm pressurized bonnet head has been adopted for the European Extremely Large Telescope (E-ELT) [3]. Utilization of a more rigid tool head [4] and multi-jet polishing [5] have also been attempted.

Combining form generation and surface smoothing into a single processing chain [6] is yet another way of increasing the overall manufacturing process efficiency.

Higher polishing efficiency can also be achieved by minimizing the total dwell time [8–10]. This includes optimizing the dwell time algorithm to minimize the total dwell time [8] and substituting the position-based dwell time implementation by a velocity feed scheme [9,10].

Because a single dwell time control mechanism (e.g., work-piece rotation) cannot support multiple independent dwell time schedules for different tool sizes targeting different spatial frequency errors, computer controlled optical surfacing (CCOS) runs have been required to be executed in an inefficient, one-at-a-time mode. In fact, the polishing efficiency can be further improved if multiple polishing tools are used simultaneously in a single polishing process. It is critical to understand that this is different from a simultaneous simulation topic [11] and enables a multiplexed physical polishing process. For instance, the large polishing machine (LPM) at the University of Arizona consists of two tools (i.e., Tool₁ and Tool₂) with different sizes. However, they have been working independently in serial runs or simultaneously on two physically separated mirrors (e.g., monolithic LSST primary-tertiary mirror, as shown in Fig. 1). This brings the potential to accelerate the polishing process by multiplexing two polishing runs figuring a single optical surface in parallel.

In our previous work [11], a non-sequential optimization technique was proposed to simultaneously optimize the dwell times and tool sizes. The deterministic figuring ability of the LPM shown in Fig. 1 has been verified through excellent matching between predicted and measured removal maps. However, the actual polishing process has been implemented sequentially, which often started with larger tools and finished with smaller tools. A significant remaining challenge is not enhancing deterministic removal using polishing parameter control, but multiplexing polishing programs and sequences into a single run, which is a pure algorithm-level innovation.

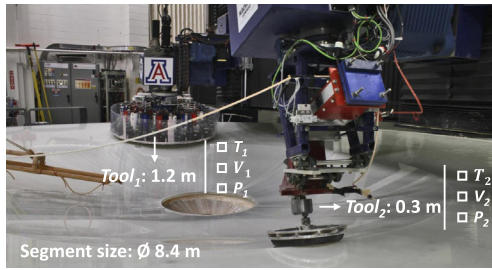


Fig. 1. Large polishing machine (LPM) with dual tools for 8.4 m class mirror manufacturing at the University of Arizona.

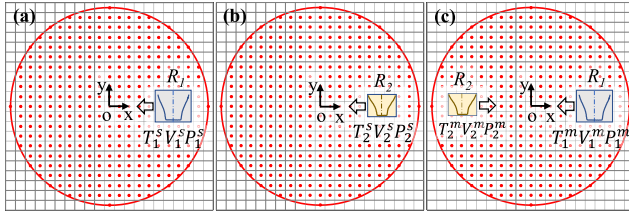


Fig. 2. Schematic TIF models comparing (a), (b) two sequential single-tool runs and (c) a multiplexed^m dual-tool run.

In the rest of this Letter, we present a multiplexed dual-tool deterministic polishing model that enables running the two polishing heads equipped on the LPM in parallel. The dwell time calculated for each individual tool is synchronized in real time under certain boundary conditions (BCs). The run velocities of the two tools are coordinated by a velocity adjustment algorithm (VAA), ensuring that the velocities are always within the affordable speed range for both tools. Also, appropriate tool paths for the dual-tool scenario are carefully studied.

The convolution-based removal model of an individual tool in Fig. 1 is defined as

$$Z(x, y) = R(u, v) ** [T(x, y) \times V(x, y) \times P(x, y)], \quad (1)$$

where “**” represents the two-dimensional convolution operator; $Z(x, y)$ is the removed material, which is equal to the convolution between the basic tool influence function (TIF), $R(u, v)$, defined in its local coordinate system, and the product of the dwell time, $T(x, y)$, the tool stroke velocity, $V(x, y)$, and the contact pressure, $P(x, y)$ of the tool. Figure 2 schematically illustrates the concepts and relationship of the single-tool and the dual-tool polishing models defined in a global Cartesian grid coordinate system. Given the optimized [8–10] sequential run parameters, which are the T_1^s , V_1^s , and P_1^s for Tool₁ and T_2^s , V_2^s , and P_2^s for Tool₂, the corresponding T_1^m , V_1^m , P_1^m , T_2^m , V_2^m , and P_2^m need to be multiplexed and synchronized for the dual-tool model.

To solve the dual-tool parameters, the relationship between the single-tool and the dual-tool models should be established. This relationship is the removed material at a certain point (x, y) and has to be identical in both cases. Therefore, the following fundamental BC (BC-1) is defined as follows:

$$\text{BC-1: } Z_1^s(x, y) \equiv Z_1^m(x, y) \quad \text{and} \quad Z_2^s(x, y) \equiv Z_2^m(x, y), \quad (2)$$

where $Z_1^s(x, y)$ and $Z_2^s(x, y)$ are the material removed by R_1 and R_2 at (x, y) in the single-tool model, respectively, and $Z_1^m(x, y)$ and $Z_2^m(x, y)$ are the material removed by R_1 and R_2 at (x, y) in the dual-tool model, respectively. Since R_1 and R_2 remain invariant, Eq. (2) can be further transformed into

$$\begin{aligned} T_1^s \times V_1^s \times P_1^s &= T_1^m \times V_1^m \times P_1^m, \\ T_2^s \times V_2^s \times P_2^s &= T_2^m \times V_2^m \times P_2^m. \end{aligned} \quad (3)$$

In addition, as a machine-specific BC, the simultaneous run of the two tools requires 180° out of phase dwell time for the LPM configuration, which has two tools translating on the $+x$ (Tool₁) and $-x$ (Tool₂) axes, as shown in Fig. 2(c), during the mirror rotation for dwell time modulation. First, one tool (e.g., Tool₁) is set as the primary tool so that its dwell time and velocities remain invariant, i.e.,

$$\begin{aligned} T_1^s(x, y) &= T_1^m(x, y), \\ V_1^s(x, y) &= V_1^m(x, y). \end{aligned} \quad (4)$$

Then, as shown in Fig. 2(c), during simultaneous polishing, Tool₁ and Tool₂ are placed at the opposite location (180°), and T_2^m is calculated with the machine-specific BC (BC-2) as

$$\text{BC-2: } T_2^m(x, y) \equiv \text{rotate}(T_1^m(x, y), 180^\circ). \quad (5)$$

It is worth mentioning that the separation angle between Tool₁ and Tool₂ can be arbitrary. The 180° is just the most convenient angle to implement the dual-tool model under the LPM's specific gantry-type configuration. Based on Eqs. (4) and (5), V_2^m is determined as

$$V_2^m(x, y) = V_2^s(x, y) \frac{T_2^s(x, y)}{T_2^m(x, y)}. \quad (6)$$

If the simultaneous cases keep their nominal pressures, which are often set as constants, all of the parameters for the dual-tool model are now synchronized. However, $V_2^m(x, y)$ obtained from Eq. (6) may exceed the maximum speed limit of the polishing machine. Therefore, the VAA shown in Algorithm 1 is employed to constrain the velocities under the valid range. The VAA adjusts the velocities in two loops. In the first loop (Lines 3–6), $V_2^m(x, y)$ is clamped to V_2^{max} if it is over the range, and the $T_2^m(x, y)$ is calculated accordingly. Afterwards, T_1^m and V_1^m are updated using Eqs. (5) and (6). In the second loop (Lines 9–12), the same operations are applied to the new $V_1^m(x, y)$, after which both V_1^m and V_2^m are guaranteed to be within the max velocity limits. Note that it is also possible to hold the velocities constant and tune the contact pressures. For most cases, contact pressure has a small dynamic range (i.e., the ratio of maximum and minimum pressure) compared to stroke velocity. Also, the removal depth is often nonlinear with respect to the very low pressure range. Therefore, we select the velocities as the main variables (and the pressures as the secondary variables) in the following case study.

The LPM adopts a turntable motion. As shown in Fig. 3, the tool path is implemented as a spiral track with respect to the center of the work piece. Equal angle and equal arc length are common types of spiral tool path control sampling methods in CCOS. For an equal-angle sampling path, since the inner dwell points are much closer than the outer ones, the dwell time per point on an inner ring is shorter than that on an outer ring when

Algorithm 1. Velocity Adjustment Algorithm

```

1: procedure: VAA ( $V_1^m, V_2^m, T_1^m, T_2^m$ )
2: [ $m, n$ ]  $\leftarrow$  [rows ( $V_1^m$ ), cols ( $V_1^m$ )]
3: while  $y < m$  and  $x < n$  do  $\triangleright$  Adjust  $V_2^m$  and  $T_2^m$ 
4:   if  $V_2^m(x, y) > V_2^{\max}$  then
5:      $V_2^m(x, y) \leftarrow V_2^{\max}$ 
6:      $T_2^m(x, y) = T_2^s(x, y) \times V_2^s(x, y) / V_2^m(x, y)$ 
7:    $T_1^m \leftarrow \text{rotate}(T_2^m, 180^\circ)$   $\triangleright$  Eq. (5)
8:    $V_1^m \leftarrow V_1^s \times T_1^s / T_1^m$   $\triangleright$  Eq. (6)
9:   while  $y < m$  and  $x < n$  do  $\triangleright$  Adjust  $V_1^m$  and  $T_1^m$ 
10:    if  $V_1^m(x, y) > V_1^{\max}$  then
11:       $V_1^m(x, y) \leftarrow V_1^{\max}$ 
12:       $T_1^m(x, y) = T_1^s(x, y) \times V_1^s(x, y) / V_1^m(x, y)$ 
13:     $T_2^m \leftarrow \text{rotate}(T_1^m, 180^\circ)$   $\triangleright$  Eq. (5)
14:     $V_2^m \leftarrow V_2^s \times T_2^s / T_2^m$   $\triangleright$  Eq. (6)

```

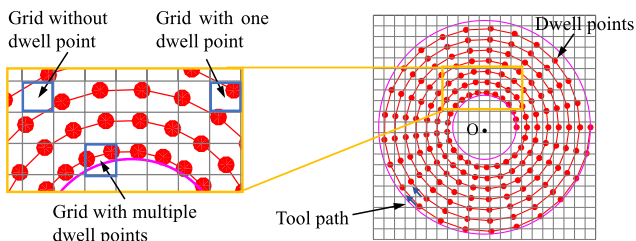


Fig. 3. Three cases of the dwell time reassignment process from original dwell time grid to actual spiral tool path.

the same amount of material is removed. On the other hand, the equal-arc-length path keeps equal arc lengths between adjacent dwell points, varying the mirror rotation speeds between dwell points on the inner and outer rings. Thus, the feed speeds need to be adjusted accordingly. Regardless of the types of spiral tool paths, the dwell time calculated for the Cartesian grid points (see Fig. 2) needs to be converted to the spiral sampling. Since the sampling of the spiral path is non-uniform and does not exactly match the original grid points, a reassignment process is performed in three different cases: (1) if no spiral sampling point is in the grid, the grid's dwell time is assigned to its nearest spiral point; (2) if only one spiral point falls in the grid, the grid's dwell time is directly assigned to this point; and (3) if multiple spiral points are in the grid, the grid's dwell time is evenly distributed to these points (see Fig. 3).

For the dual-tool multiplexing model, as shown in Fig. 4, the tools can be fed in two modes, one is in-out and the other is in-in. In the in-out method [see Fig. 4(a)], Tool₁ and Tool₂ move in the same direction so that tool collision is avoided. This is generally applicable to any dual-tool polishing scenario. When polishing a mirror with a central obscuration, e.g., the GMT on-axis segment, the in-in feed mode [see Fig. 4(b)] can also be applied, since the tool collision problem is automatically resolved due to the hole at the mirror's center. In this study, the performances of applying the two-tool feed modes on the two aforementioned types of spiral paths are studied and demonstrated via a simulation based on a real \varnothing 8.4 m GMT segment polishing configuration.

Figure 5 presents the simulated initial surface error map. The single-tool parameters in Eq. (1) for Tool₁ and Tool₂ are simulated using Zernike coefficients. The TIF sizes of R_1 and R_2 are

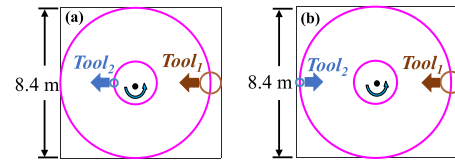


Fig. 4. (a) In-out and (b) in-in feed modes for multiplexed dual-tool polishing model.

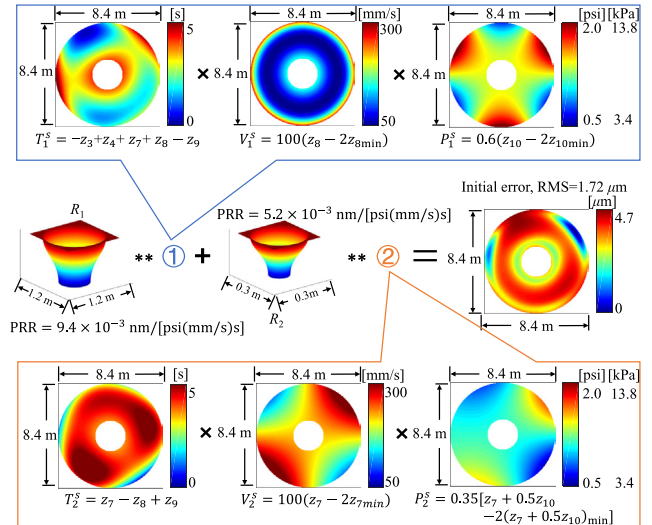


Fig. 5. Synthetic GMT segment surface error map, peak removal rate; z_n , the " n " th Zernike coefficient.

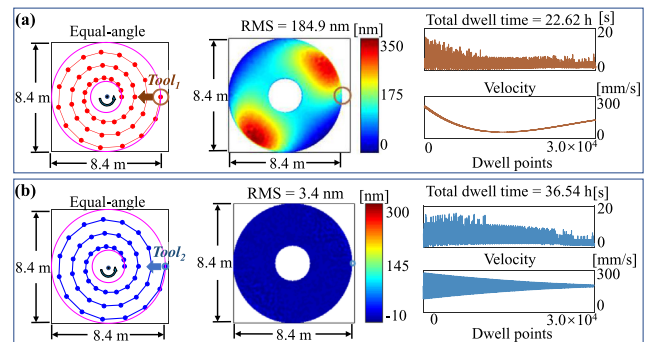


Fig. 6. CCOS case study of two sequential single-tool runs using (a) Tool₁ followed by (b) Tool₂ (Visualization 1).

modeled to \varnothing 1.2 m and \varnothing 0.3 m, respectively, considering their effective tool contact area and orbital stroke motion. As a benchmark, the results of the sequential two single-tool runs are given in Fig. 6. In Fig. 6(a), the figure error is reduced from 1.72 μ m to 184.9 nm RMS after processing with Tool₁. The residual figure error is then further processed by Tool₂ [see Fig. 6(b)], and the final residual is 3.4 nm RMS. The total dwell time required to achieve this residual error is 22.62 + 36.54 = 59.16 h.

In the multiplexed dual-tool case, Tool₁ is selected as the *primary tool* so that the parameters of Tool₂ (i.e., the dwell time and velocities) are adjusted and synchronized with those of Tool₁. The performances of the in-in and the in-out feed modes with the equal-angle paths are first studied in Figs. 7(a) and 7(b), respectively. Both of the feed modes with constant angular speed

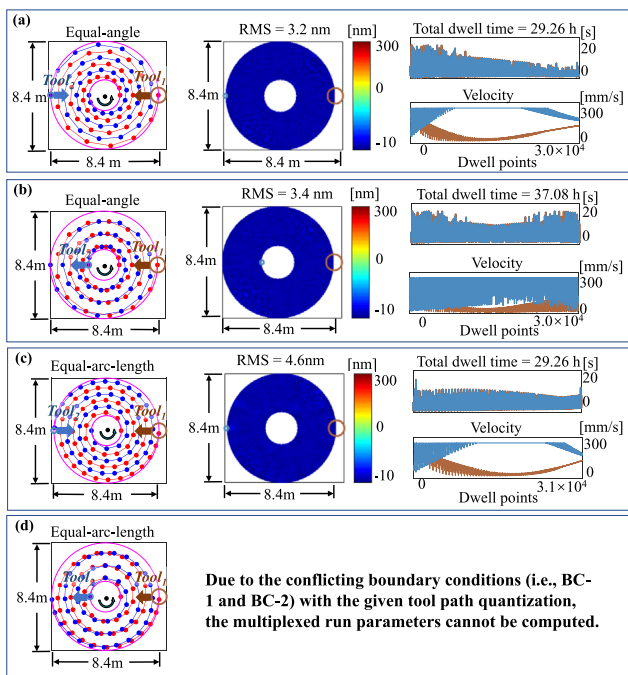


Fig. 7. Case study simulations using dual-tool CCOS multiplexing model: (a) in-in feed with equal-angle path (Visualization 2), (b) in-out feed with equal-angle path (Visualization 3), (c) in-in feed with equal-arc-length path (Visualization 4), and (d) in-out feed with equal-arc-length path.

achieve similar residual errors, namely, 3.2 nm and 3.4 nm RMS, respectively. The VAA has adjusted the velocities for Tool₁ and Tool₂ to be within their respective maximum speeds. It is worth noting that, in practice, the linear-shift-invariant range of the TIF depends on the specific run configuration, such as polishing pads, tool types, and polishing slurry. It can also be observed that when the in-in feed mode is used [see Fig. 7(a)], as the tools move toward the center, the density of the dwell points increases, and the dwell time distributed to each dwell point becomes shorter.

The in-in feed mode shows shorter dwell time (29.26 h) than the in-out feed mode (37.08 h), almost 21% less. Compared with the 59.16 h two sequential single-tool runs, the multiplexed polishing efficiency is significantly improved by 50.54% with the in-in mode. The reason for the lower polishing efficiency of the in-out mode is that, as Tool₁ moves toward the center, dwell points become more dense, resulting in shorter $T_1^m(x, y)$. The $T_2^m(x, y)$ also become shorter according to Eq. (5). Therefore, based on Eq. (6), $V_2^m(x, y)$ should increase. However, if $V_2^m(x, y)$ are already large, the VAA may clamp $V_2^m(x, y)$ to V_2^{\max} , which in turn causes the corresponding $T_2^m(x, y)$ to increase, leading to higher total dwell time.

Figures 7(c) and 7(d) further demonstrate the results of the two feed modes with the equal-arc-length paths. The in-in feed mode shown in Fig. 7(c) achieves a similar residual error at 4.6 nm RMS, while the total dwell time of 29.26 h is similar to that calculated using the same feed mode applied with the equal-angle path shown in Fig. 7(a).

The in-out feed mode shown in Fig. 7(d), however, cannot be applied with the equal-arc-length path. In the in-out feed mode, at any instant, Tool₁ and Tool₂ will have different radial positions with respect to the center of mirror rotation so that the arc

lengths cannot be equal. This mode is thus not suitable for the equal-arc-length path. On the contrary, in the in-in feed mode, both tools have the same radial position at any time so that the equal-arc-length condition can be guaranteed. Therefore, the equal-arc-length path is only applicable to the in-in feed mode.

Finally, we can conclude from Fig. 7, that all of the multiplexed dual-tool models (in Fig. 7) for the 8.4 m GMT polishing case study achieves significantly enhanced fabrication efficiency in terms of total dwell time while maintaining the final surface figure of the original sequential dwell time optimization. For general applications, where tool collision should be considered, and the in-in feed mode cannot be employed, the dual-tool multiplexing theory and BCs can still be efficiently implemented with the in-out feed mode with an equal-angle path shown in Fig. 7(b).

In this Letter, we proposed a multiplexed dual-tool deterministic polishing model that enables the efficient polishing of large optics using two tools in parallel. It is critical to note that this is a purely algorithm-based innovation. All of the deterministic removal processes (e.g., Bonnet tool, magnetorheological finishing, stressed lap, non-Newtonian lap) and various dwell time optimization algorithms are still essential building blocks enabling this CCOS multiplexing. Two dwell time maps using any existing optimization methods can be directly multiplexed. Setting one tool as the primary tool, the dwell time and the velocities of the two tools are synchronized based on certain BCs and VAA. The GMT polishing case study results demonstrate that the proposed dual-tool model improves the single-tool polishing efficiency by a factor of up to 50.54%, while the final surface error is not affected, which proves the effectiveness of the proposed multiplexing theory. The dual-tool model can be extended to an N -tool model multiplexing N tools, in which case the polishing efficiency can be further improved.

Funding. Technology Research Initiative Fund Optics/Imaging Program, University of Arizona, USA; Natural Science Foundation of Fujian Province, China (2018J01528).

Disclosures. The authors declare no conflicts of interest.

REFERENCES

- L. R. Graves, G. A. Smith, D. Apai, and D. W. Kim, *Nanomanufacturing Metrol.* **2**, 65 (2019).
- S. West, R. Angel, B. Cuerden, W. Davison, J. Hagen, H. Martin, D. W. Kim, and B. Sisk, in *Optical Fabrication and Testing* (Optical Society of America, 2014), paper OTh2B-4.
- G. Yu, D. D. Walker, and H. Li, *Proc. SPIE* **8416**, 841602 (2012).
- C. Wang, Z. Wang, Q. Wang, X. Ke, B. Zhong, Y. Guo, and Q. Xu, *Int. J. Adv. Manuf. Technol.* **88**, 1607 (2017).
- C. Wang, C. Cheung, L. Ho, M. Liu, and W. Lee, *Int. J. Mach. Tools Manuf.* **115**, 60 (2017).
- X. Su, P. Ji, K. Liu, D. Walker, G. Yu, H. Li, D. Li, and B. Wang, *Opt. Express* **27**, 17979 (2019).
- D. W. Kim, J. H. Burge, J. M. Davis, H. M. Martin, M. T. Tuell, L. R. Graves, and S. C. West, *Proc. SPIE* **9912**, 99120p (2016).
- T. Wang, L. Huang, H. Kang, H. Choi, D. W. Kim, K. Tayabaly, and M. Idir, *Sci. Rep.* **10**, 1 (2020).
- L. Zhou, Y. Dai, X. Xie, X. Peng, F. Shi, and S. Li, in *EUSPEN's 16th International Conference & Exhibition* (2016).
- T. Wang, L. Huang, Y. Zhu, M. Vescovi, D. Khune, H. Kang, H. Choi, D. W. Kim, K. Tayabaly, and N. Bouet, *Appl. Opt.* **59**, 3306 (2020).
- D. W. Kim, S.-W. Kim, and J. H. Burge, *Opt. Express* **17**, 21850 (2009).